Geophysical Research Letters

Supporting Information for

Wildfire impact on environmental thermodynamics and severe convective storms

Yuwei Zhang[1,3], Jiwen Fan[1,*], Timothy Logan[2], Zhanqing Li[3], Cameron R. Homeyer[4]

1 Atmospheric Sciences and Global Change Division, Pacific Northwest National Laboratory, Richland, WA 99352

2 Department of Atmospheric Sciences, Texas A&M University, College Station, TX 77843

3 Department of Atmospheric and Oceanic Science, University of Maryland, College Park, MD 20742

[4] School of Meteorology, University of Oklahoma, Norman, OK 73072

Corresponding author: Jiwen Fan (Jiwen.Fan@pnnl.gov)

Contents of this file

Supplementary text

Figures S1 to S8

Introduction

The supplementary text includes some detail description about model development, WRF-Chem model configurations and simulations, the observational datasets used for model evaluation, and the references cited in this document. Description of Figures S1-S8 are shown in the corresponding figure caption.

Supplementary text

Description of model development

For the model development, we provide more details about biomass emissions, fire location, timing, plume height, etc. The hourly biomass emission, active fire location, and burning area were obtained from the Fire INventory from NCAR (FINN) model (Wiedinmyer et al., 2011). The location and timing for the fires are identified globally using the MODIS Thermal Anomalies Product. The Global Land Cover Characteristics 2000 dataset and the MODIS Vegetation Continuous Fields Product were used to determine the burned area for each vegetation type based on percentage vegetative cover in each 1 km^2 fire pixel. The FINN data is then interpolated to the host model grid. For grid points with fire according to FINN, the sub-grid plume rise model is driven by the environmental dynamics from the atmosphere model in WRF-Chem and the plume dynamics are estimated based on fire information from FINN (Freitas et al., 2007). The final height of the plume is then used in the source emission field of the host model to determine the effective injection height where heat and aerosols emitted during the flaming phase would be released and interact with the atmosphere circulation and transport. The aerosol emission from the fire is added as described in Grell et al. (2011).

The sensible heat flux from the subgrid plume model is input to the atmosphere as an additional source term in the equation for potential temperature θ, equal to the vertical divergence of the heat flux,

$$\frac{d(\mu\theta)}{dt}(x,y,z) = R_{\Theta}(\Phi) + \frac{\mu(x,y)\phi_h(x,y)}{\sigma\rho(x,y,z)}\frac{\partial}{\partial z} exp\left(-\frac{z}{z_{ext}}\right) \qquad \textbf{(1)}$$

where μ(x,y) is the hydrostatic component of the pressure differential of dry air between the surface and the top of the domain, $R_{\Theta}(\Phi)$ is the component of the source term (commonly called "tendency" in WRF) in the atmospheric model thermodynamic equation, σ is the specific heat of the air, ρ(x,y,z) is the density, and z_{ext} is the heat extinction depth (Mandel et al. 2011).

Model configurations and simulations

For the evaluation of the improved WRF-Chem model at 3-km resolution for wildfires without pyroCb, we run the WRF-Chem simulations of wildfires over the central United States from 1200 UTC 15 July to 1200 UTC 19 July 2016. The simulated domain is shown in Fig S1a with 65 vertical levels. We used the Model for Simulating Aerosol Interactions and Chemistry (MOSAIC) aerosol model with four bins (Zaveri et al., 2008). The physics schemes applied in the simulation are the Unified Noah land surface scheme (Chen and Dudhia, 2001), Yonsei University planetary boundary layer scheme (Hong et al., 2006), the rapid radiative transfer model for general circulation model (RRTMG) longwave and shortwave radiation schemes (Iacono et al., 2008), and Morrison two-moment microphysics scheme (Morrison et al., 2005) with the hail option. The initial and lateral boundary conditions for the meteorological fields were produced from the Rapid

Refresh (RAP) model that is comprised primarily of a numerical forecast model and an analysis/assimilation system at 13-km resolution (Benjamin et al. 2016). The chemical lateral boundary and initial conditions were created from the Modern-Era Retrospective analysis for Research and Applications, Version 2 (MERRA-2, Gelaro et al., 2017). The meteorological field was reinitialized every 30 hours with the RAP data. The anthropogenic emission was from NEI-2011 emissions. The biogenic emission came from the Model of Emissions of Gases and Aerosols from Nature (MEGAN) product (Guenther et al., 2006). To evaluate the temperature profiles on 18 July 2016, we use the sounding data from the National Oceanic and Atmospheric Administration / Earth System Research Laboratory ((NOAA/ESRL) radiosonde database.

To evaluate Wildfire with the new plume model development, WRF-Chem-SFIRE is run, which uses the similar model configuration as Wildfire. The inner fuel model for fire in WRF-Chem-SFIRE uses a resolution of 50 meters that is 20 times finer than the atmospheric model grid. The Anderson 13 fuel category data and high-resolution topography data available at http://www.landfire.gov are used in SFIRE for estimating fire behavior and spread.

Description of datasets used for model evaluation

The maximum hail sizes from the simulations are estimated using a physically-based hail forecasting model (HAILCAST), which is online coupled with WRF-Chem simulations (Adams-Selin and Ziegler, 2016). HAILCAST forecasts the maximum expected hail diameter at the surface using updraft and microphysical information produced by WRF-Chem. We incorporate the most updated HAILCAST version from WRF v4.0 (Adams-Selin et al., 2018) into the WRF-Chem V3.9.1 for this study. The prediction of lightning activity from model simulations is estimated with the utilization of the lightning potential index (LPI) described in Yair et al. (2010). The smoke plume height data digitized from the Multi-angle Imaging Spectro Radiometer (MISR) based on the MISR INteractive eXplorer (MINX) software are utilized to evaluate the predicted plume height (Nelson et al., 2014). To analyze and evaluate the thermodynamics before the convection, sounding data from National Weather Service forecast office at Amarillo, TX (KAMA) is used. The observed radar reflectivity and the radar-retrieved maximum expected size of hail (MESH) data are from Gridded NEXRAD WSR-88D Radar data (GridRad; Homeyer and Bowman, 2017) created at 5-min temporal intervals for this study. The MESH data used in this study are developed from a newly-improved algorithm (Murillo and Homeyer, 2019). The National Centers for Environmental Prediction /Environmental Modeling Center ((NCEP/EMC) Stage IV Data is used as the observation of precipitation with hourly output at 4-km resolution (Lin and Mitchell, 2005). The lightning observation data are from National Lightning Detection Network (NLDN; Cummins and Murphy, 2009).

References

Chen, F, and J. Dudhia (2001) Coupling an advanced land surface–hydrology model with the Penn State–NCAR MM5 modeling system. Part I: Model implementation and sensitivity. *Mon Weather Rev* 129(4):569–585.

Cummins, K. L., & Murphy, M. J. (2009). An overview of lightning locating systems: History, techniques, and data uses, with an in-depth look at the U.S. NLDN. *IEEE Transactions on Electromagnetic Compatibility*, 51(3), 499–518.

Gelaro, R, McCarty W, Suárez MJ, Todling R, Molod A, Takacs L, Randles CA, Darmenov A, Bosilovich MG, Reichle R, Wargan K, et al., (2017), The modern-era retrospective analysis for research and applications, version 2 (MERRA-2). *J. Clim.,* 30(14):5419–5454

Guenther, A., T. Karl, P. Harley, C. Wiedinmyer, P. I. Palmer, C. Geron (2006), Estimates of global terrestrial isoprene emissions using MEGAN (Model of Emissions of Gases and Aerosols from Nature), *Atmos. Chem. Phys.,* 6, 3181-3210.

Hong, S-Y, Y. Noh, J. Dudhia (2006), A new vertical diffusion package with an explicit treatment of entrainment processes. *Mon Weather Rev* 134(9):2318–2341.

Iacono, M.J, et al. (2008), Radiative forcing by long-lived greenhouse gases: Calculations with the AER radiative transfer models. *J Geophys Res* 113(D13):D13103.

Morrison, H., J. A. Curry, and V. I. Khvorostyanov (2005), A new double moment microphysics parameterization for application in cloud and climate models. Part I: Description, *J. Atmos. Sci.*, 62(6), 1665–1677.

Westerling, A. L., H. G. Hidalgo, D. R. Cayan, and T. W. Swetnam (2006), Warming and earlier spring increase Western U.S. forest wildfire activity, *Science,* 313 (5789), 940–943.

Wiedinmyer, C., Akagi, S. K., Yokelson, R. J., Emmons, L. K., Al-Saadi, J. A.,Orlando, J. J., and Soja, A. J. (2011), The Fire INventory from NCAR (FINN): a high resolution global model to estimate the emissions from open burning, *Geosci. Model Dev.,* 4, 625-641, doi:10.5194/gmd-4-625-2011.

Zaveri, R. A., R. C. Easter, J. D. Fast, and L. K. Peters, (2008), Model for Simulating Aerosol Interactions and Chemistry (MOSAIC). United States: N. p., 2008. Web. doi:10.1029/2007JD008782.

Figures S1 to S8

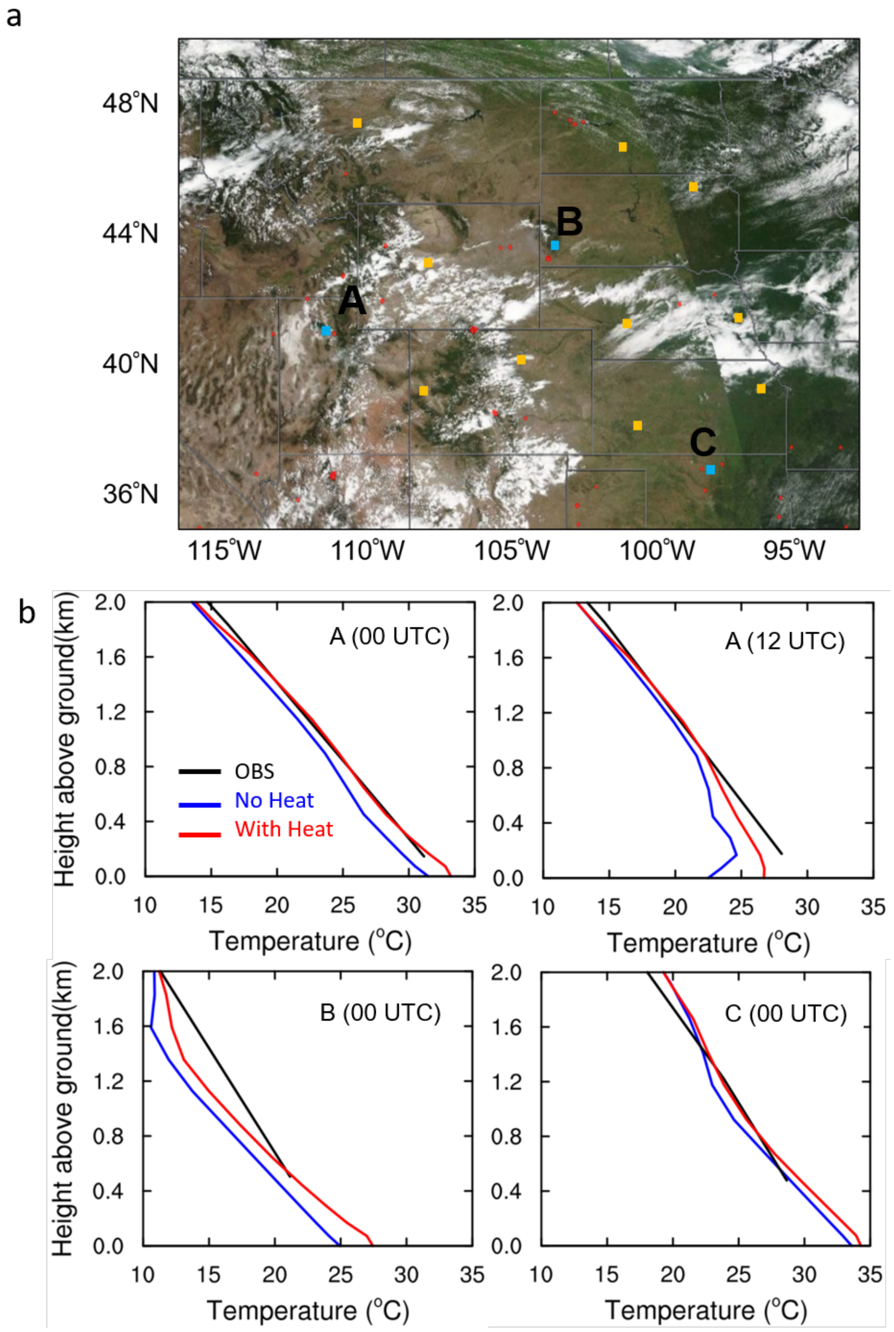

Figure S1 (a) True Color image and Fires/Thermal Anomalies (red dots) from Suomi NPP/ VIIRS and NOAA/ESRL Radiosonde stations (blue or yellow squares) in the simulated domain on 17 July 2016, (b) Temperature profiles from the observation (black), the simulation with the original WRF-Chem (blue) and the simulation from the improved WRF-Chem with heat flux accounted (red) for three sounding stations close to fires (blue squares in a) on 18 July 2016. Other stations did not have measurements obviously influenced by wildfires.

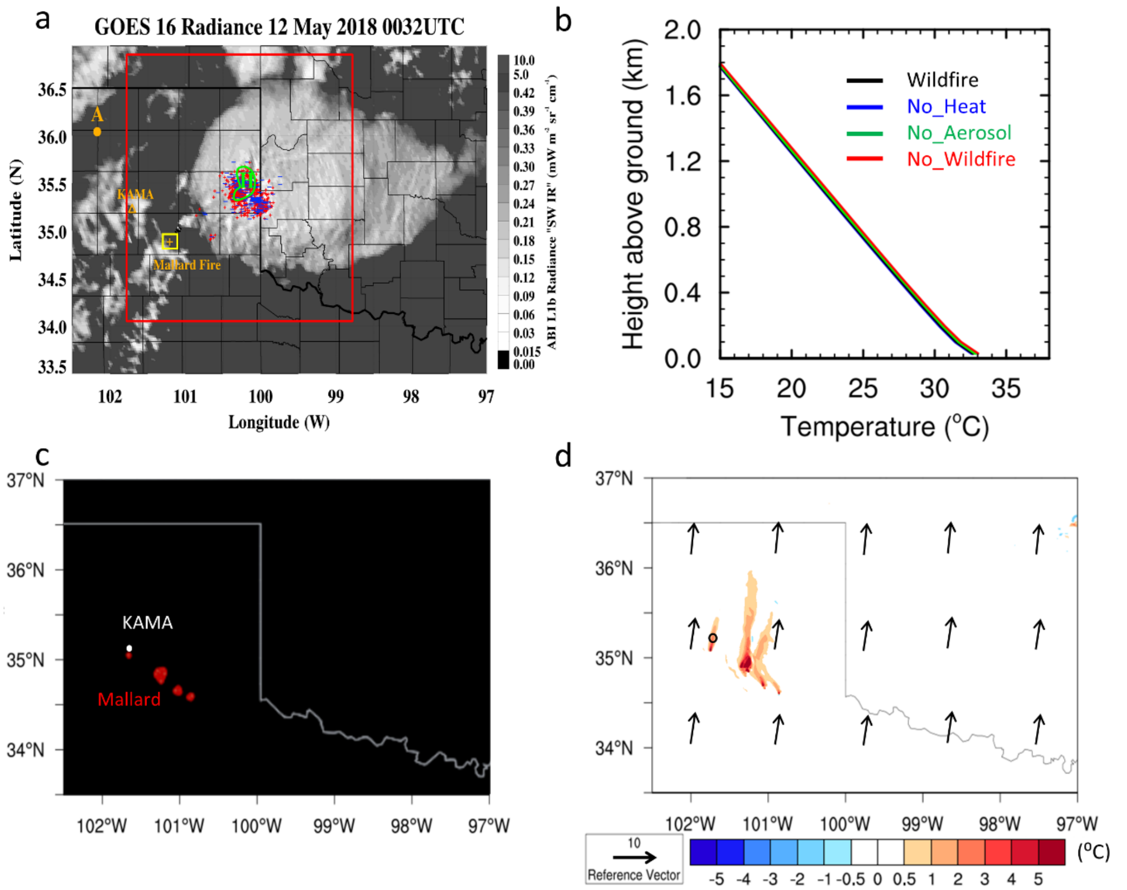

Figure S2 (a) The pyroCb observed from GOES-16 Band 7 ("shortwave window" Infrared) and the lightning flashes (marked as "+") from the National Lightning Detection Network (NLDN) at 0032 UTC 12 May 2018, and the area of observed hail (green contour line) from the MESH data at 0030 UTC. The location of A is a site that was not influenced by wildfire and KAMA is a sounding site. The latitude and longitude ranges of (a) show the model simulation domain. The red box is the study domain for analysis of convection. The yellow box is for the analysis of temperature and moisture profiles over the Mallard fire area shown in Figure 1g, h. (b) Profile of temperature at 0000 UTC 11 May at the site A from the simulations. (c) Fire location detected by MODIS Thermal Anomalies Product on 10 May. (d) 2-m temperature anomaly (shaded) from No_Wildfire to Wildfire and 10-m wind (arrows) in Wildfire at 0000 UTC 11 May. KAMA sounding site is marked as circle.

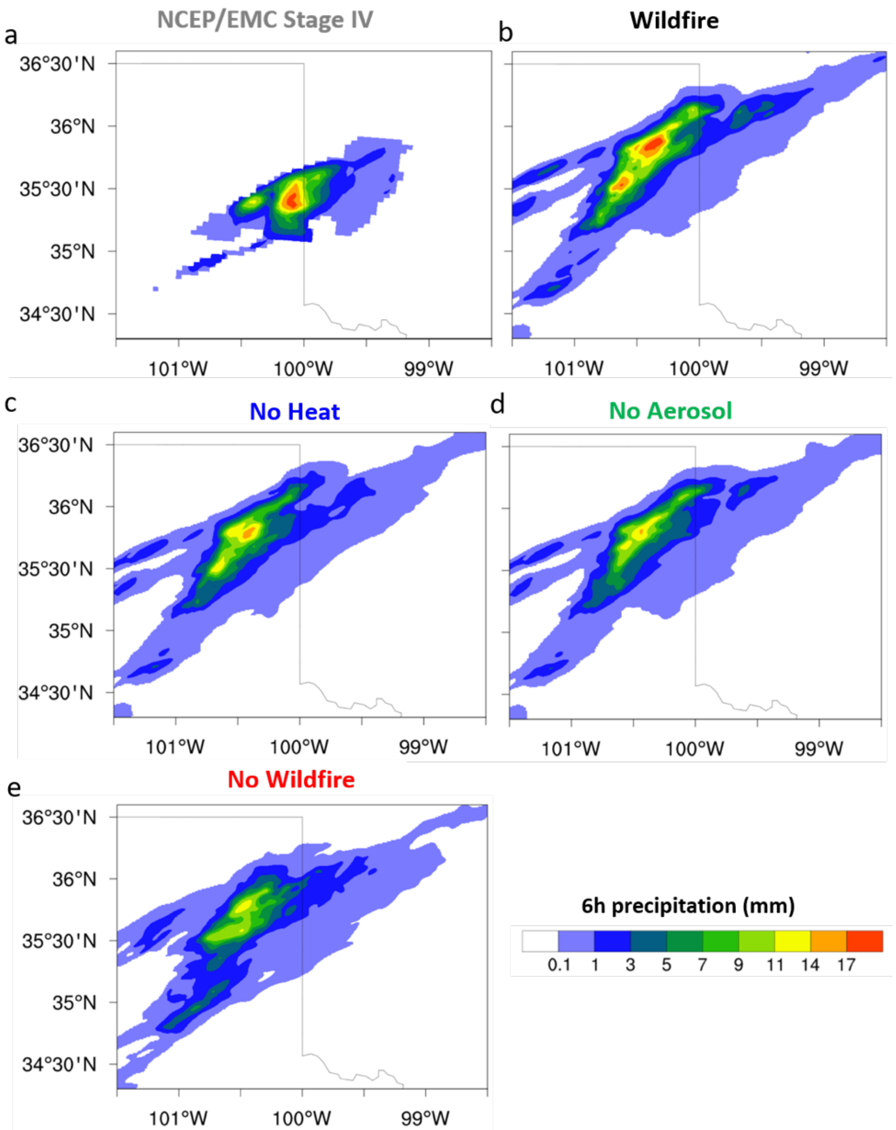

Figure S3 Accumulated precipitation from (a) NCEP/EMC Stage IV data, (b) Wildfire, (c) No_Heat, (d) No_Aerosol, and (e) No_Wildfire over a 6-h time period from 2000 UTC 11 May to 0200 UTC 12 May.

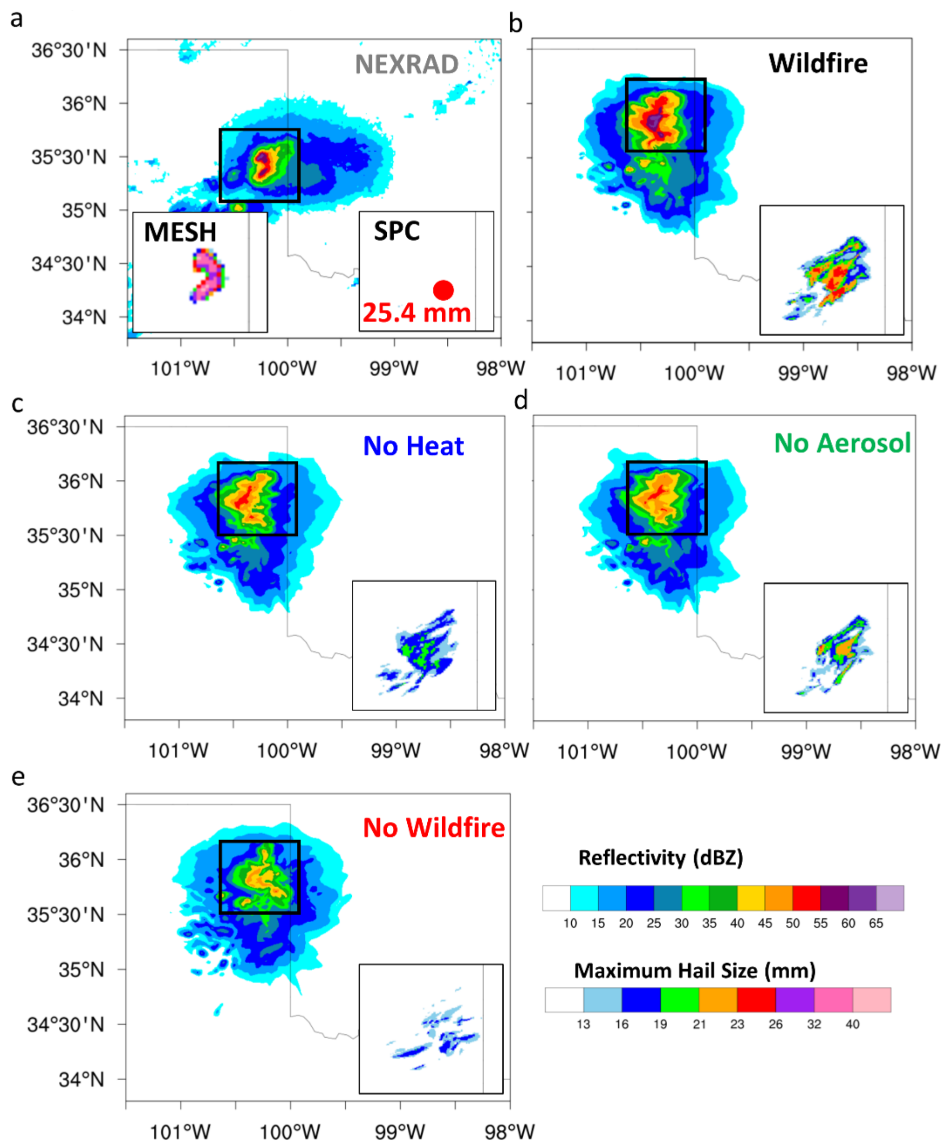

Figure S4 Composite reflectivity at the time when the maximum reflectivity is reached in temporal evolution from (a) NEXRAD at 0015 UTC 12 May, (b) Wildfire, (c) No_Heat, (d) No_Aerosol, (e) No_Wildfire at 2330 UTC 11 May. The corresponding maximum hail size is shown in the bottom-embedded small boxes for the black box region marked on the reflectivity plot. Both the SPC report and MESH data are shown on (a). The modeled results are from the HAILCAST estimation.

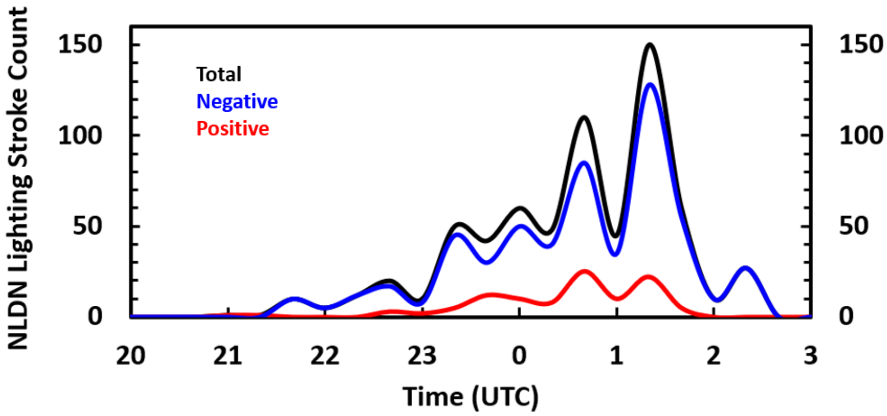

Figure S5 Time series of CG lightning stroke (flashes with all positive CG lightning greater than or equal to 15 kA) from NLDN for the Mallard pyroCb (red for the positive lightning; blue for the negative lightning, and black for total lightning).

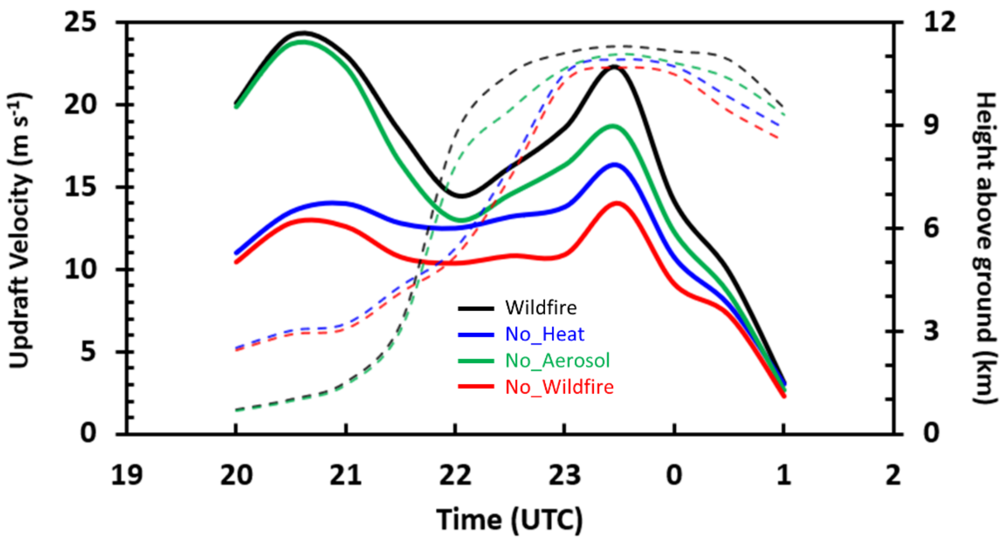

Figure S6 Time series of vertical maximum of updraft velocities (solid lines) and the corresponding altitudes above ground (dashed lines) of the averaged top 25 percentile updraft profiles for $w > 2$ m s^{-1} over the analysis domain as shown in the red box in Figure S2a from the simulation Wildfire (black), No_Heat (blue), No_Aerosol (green) and No_Wildfire (red).

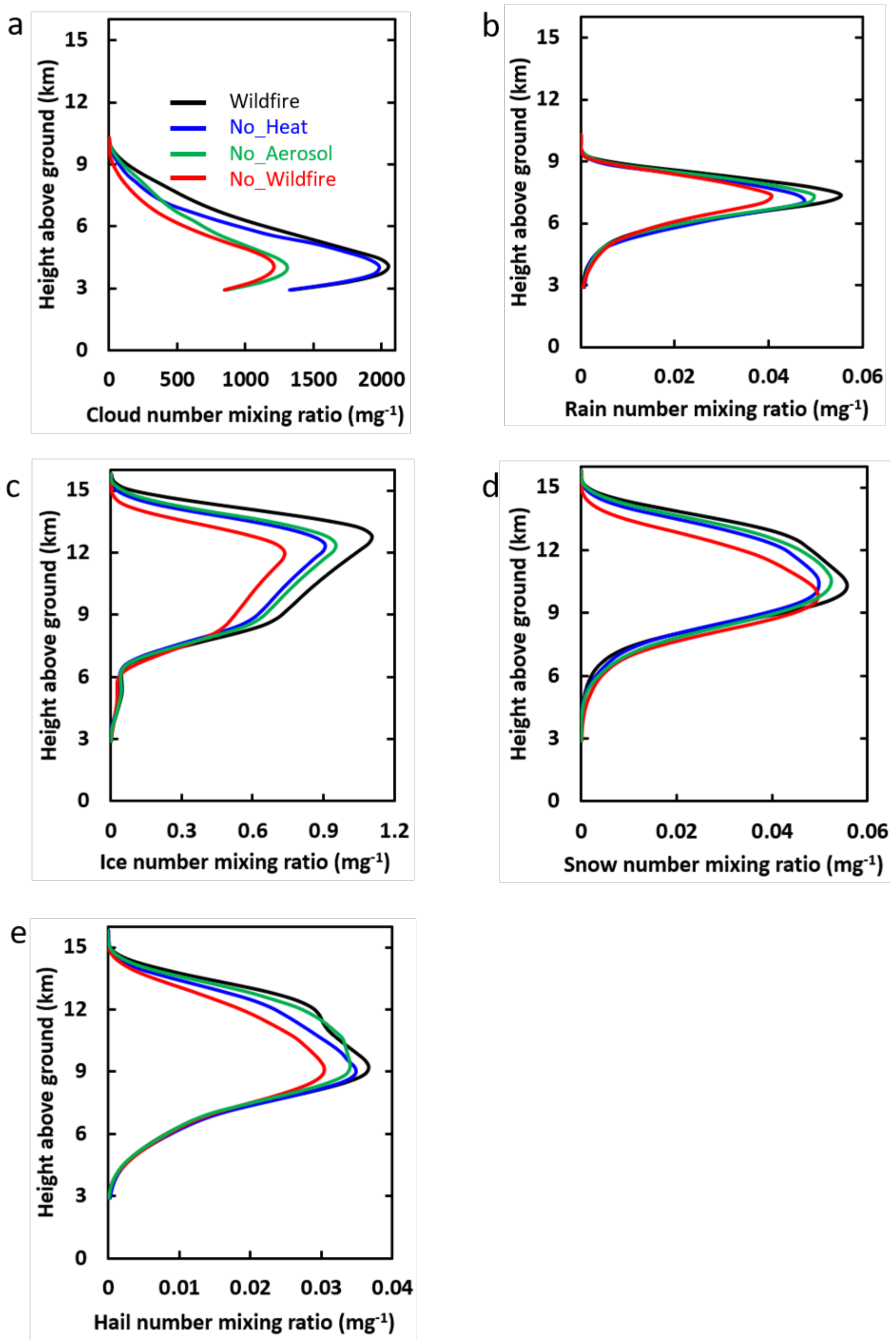

Figure S7 Vertical profiles of number mixing ratios for (a) cloud, (b) rain, (c) ice, (d) snow, and (f) hail averaged over the top 25 percentiles (i.e., 75th to 100th) of the updrafts with w>2 m s^{-1} from the simulations of Wildfire (black), No_Heat (blue), No_Aerosol (green), and No_Wildfire (red) during the strong convection period from 2300 UTC 11 May to 0000 UTC 12 May over the analysis domain as shown in the red box in Figure S2a.

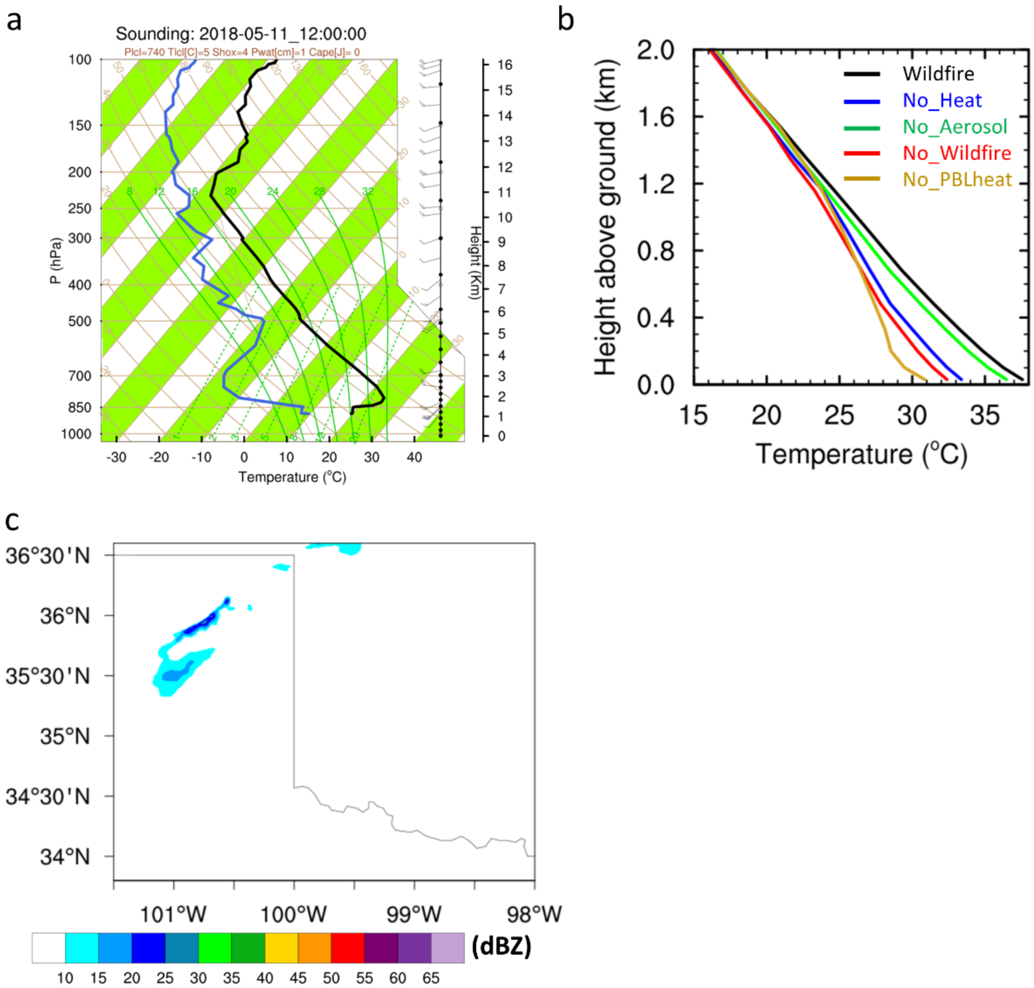

Figure S8 (a) The skew-T plot for the sounding at KAMA at 1200 UTC 11 May (~8 hours before the initiation of convection). (b) Temperature profiles of Wildfire (black), No_Heat (blue), No_Aerosol (green), No_Wildfire (red), and No_PBLheat (gold) at 1800 UTC (2-hour before the initiation of convection) 11 May at the Mallard fire region (yellow box in Figure S2a). (c) Composite reflectivity from No_PBLheat at 2330 UTC when the maximum reflectivity is reached.